Article

Quantum Chemical Approach to the Mechanism for the Biological Conversion of Tyrosine to Dopaquinone

Toshinori Inoue, Yoshihito Shiota, and Kazunari Yoshizawa

J. Am. Chem. Soc., **2008**, 130 (50), 16890-16897 • DOI: 10.1021/ja802618s • Publication Date (Web): 14 November 2008

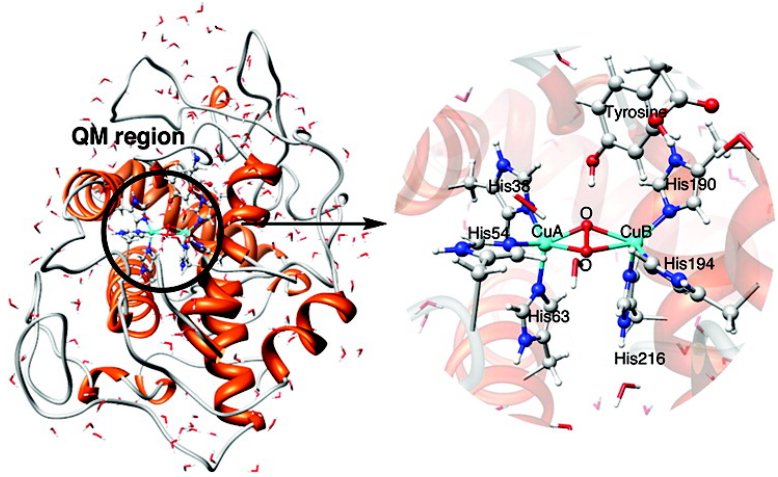

More About This Article

Additional resources and features associated with this article are available within the HTML version:

- Supporting Information
- Access to high resolution figures
- Links to articles and content related to this article
- Copyright permission to reproduce figures and/or text from this article

View the Full Text HTML

J|A|C|S
ARTICLES

Published on Web 11/14/2008

Quantum Chemical Approach to the Mechanism for the Biological Conversion of Tyrosine to Dopaquinone

Toshinori Inoue, Yoshihito Shiota, and Kazunari Yoshizawa*

Institute for Materials Chemistry and Engineering, Kyushu University, Nishi-ku, Fukuoka 819-0395, Japan

Received April 10, 2008; E-mail: kazunari@ms.ifoc.kyushu-u.ac.jp

Abstract: Tyrosinase catalyzes the biological conversion of tyrosine to dopaquinone with dioxygen at the dinuclear copper active site under physiological conditions. On the basis of the recent X-ray crystal structural analysis of tyrosinase (*J. Biol. Chem.* **2006**, *281*, 8981), a possible mechanism for the catalytic cycle of tyrosinase is proposed by using quantum mechanical/molecular mechanical calculations, which can reasonably take effects of surrounding amino-acid residues, hydrogen bonding, and protein environment into account. The (μ-η^2:η^2-peroxo)dicopper(II) species plays a role in a series of elementary processes mediated by the dicopper species of tyrosinase. A stable phenoxyl radical is involved in the reaction pathway. The catalysis has five steps of proton transfer from the phenolic O−H bond to the dioxygen moiety, O−O bond dissociation of the hydroperoxo species, C−O bond formation at an *ortho* position of the benzene ring, proton abstraction and migration mediated by His54, and quinone formation. The energy profile of the calculated reaction pathway is reasonable in energy as biological reactions that occur under physiological conditions. Detailed analyses of the energy profile demonstrate that the O−O bond dissociation is the rate-determining step. The activation energy for the O−O bond dissociation at the dicopper site is computed to be 14.9 kcal/mol, which is in good agreement with a measured kinetic constant. As proposed recently, the His54 residue, which is flexible because it is located in a loop structure in the protein, would play a role as a general base in the proton abstraction and migration in the final stages of the reaction to produce dopaquinone.

Introduction

Matoba et al.[1] recently succeeded in the crystallization of some forms of tyrosinase (EC 1.14.18.1) from *Streptomyces castaneoglobisporus* with a caddie protein (ORF378; ORF = open reading frame) and carried out X-ray crystal structural analyses at high resolutions of up to 1.2 Å. Tyrosinase, which contains dinuclear copper ions at the active site, is an essential enzyme for all organisms.[2−8] It catalyzes the conversion of tyrosine to dopaquinone (reaction 1), which is a precursor of the melanine pigment. Since melanin is a key pigment of some phenomena such as suntan, skin disorder, and bruising of fruits, tyrosinase has been attracting much attention from cosmetology, medicine, and agriculture to control synthesizing the melanin pigment.

Tyrosinase is classified into the type 3 copper protein family as well as catechol oxidase and hemocyanin. These three enzymes have very similar dicopper active sites, but their

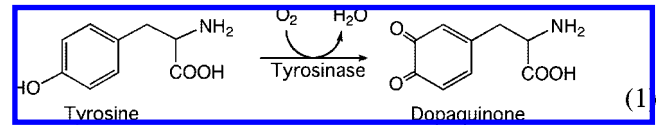

enzymatic functions are different. Tyrosinase initiates the synthesis of melamine by catalyzing the hydroxylation of monophenols to *ortho*-diphenols (cresolase activity) and the subsequent two-electron oxidation to *ortho*-quinones (catecholase activity) with dioxygen.[2] On the other hand, catechol oxidase has the catecholase activity, but lacks the cresolase activity. Hemocyanin plays the role of oxygen carrier in crustaceans like hemoglobin in mammals, but it is considered not to have any catalytic activity. These different enzymatic functions are believed to derive from accessibility to the active site. Therefore, the X-ray crystal structural analyses of tyrosinase,[1] hemocyanin,[9−11] and catechol oxidase[12,13] are essential to compare the correlation between their functions and surrounding environments of the dicopper active site. In this sense, the recent X-ray structural analysis of tyrosinase is of great use

(1) Matoba, Y.; Kumagai, T.; Yamamoto, A.; Yoshitsu, H.; Sugiyama, M. *J. Biol. Chem.* **2006**, *281*, 8981.
(2) Solomon, E. I.; Sundaram, U. M.; Machonkin, T. E. *Chem. Rev.* **1996**, *96*, 2563.
(3) Garcia-Borron, J. C.; Solano, F. *Pigm. Cell Res.* **2002**, *15*, 162.
(4) Land, E. J.; Ramsden, C. A.; Riley, P. A. *Acc. Chem. Res.* **2003**, *36*, 300.
(5) Halaouli, S.; Asther, M.; Sigoillot, J. C.; Hamdi, M.; Lomascolo, A. *J. Appl. Microbiol.* **2006**, *100*, 219.
(6) Marusek, C. M.; Trobaugh, N. M.; Flurkey, W. H.; Inlow, J. K. *J. Inorg. Biochem.* **2006**, *100*, 108.
(7) Wang, N.; Hebert, D. N. *Pigm. Cell. Res.* **2006**, *19*, 3.
(8) Claus, H.; Decker, H. *Syst. Appl. Microbiol.* **2006**, *29*, 3.
(9) Gaykema, W. P. J.; Hol, W. G. J.; Vereijken, J. M.; Soeter, N. M.; Bak, H. J.; Beintema, J. J. *Nature* **1984**, *309*, 23.
(10) Magnus, K. A.; Hazes, B.; Ton-That, H.; Bonaventura, C.; Bonaventura, J.; Hol, W. G. J. *Proteins* **1994**, *19*, 302.
(11) Cuff, M. E.; Miller, K. I.; van Holde, K. E.; Hendrickson, W. A. *J. Mol. Biol.* **1998**, *278*, 855.
(12) Klabunde, T.; Eicken, C.; Sacchettini, J. C.; Krebs, B. *Nat. Struct. Biol.* **1998**, *5*, 1084.
(13) Gerdemann, C.; Eicken, C.; Krebs, B. *Acc. Chem. Res.* **2002**, *35*, 183.

10.1021/ja802618s CCC: $40.75

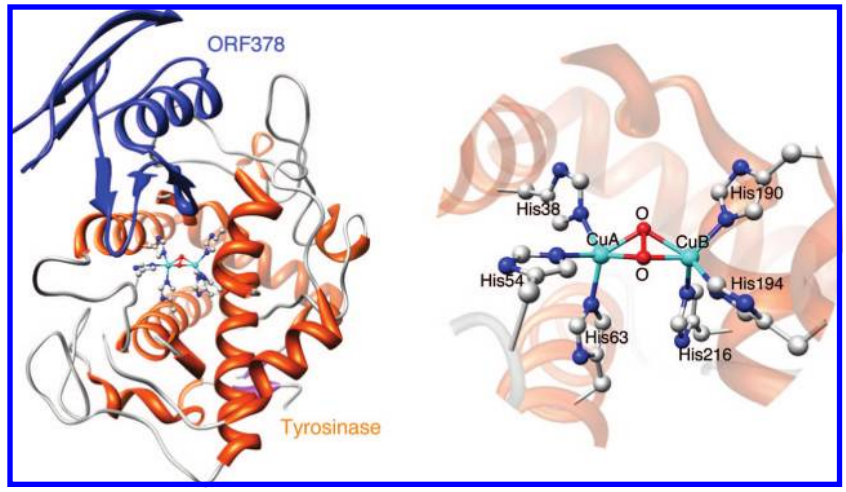

Figure 1. X-ray crystal structure of the oxy form of tyrosinase with ORF378 (blue).

to elucidate the biological mechanism for the conversion of tyrosine to dopaquinone. From spectroscopic measurements, the presence of oxy-tyrosinase, in which dioxygen is bound to the dicopper site, was demonstrated during the catalytic cycle of tyrosinase.[14] Moreover, some sequence analysis data implied that six histidine residues should exist in the active site of tyrosinase as ligands of the two copper ions.[13,15,16] Measured reaction rates of tyrosinase from kinetic analysis indicate that the oxidation of *o*-diphenols is much more rapid than the *o*-hydroxylation of monophenols ($k_{\text{oxidation}} = 10^7\ \text{s}^{-1}$, $k_{\text{hydroxylation}} = 10^3\ \text{s}^{-1}$).[17]

Dicopper model complexes that mimic the active site of the type 3 copper protein family have played an essential role to better understand the structure−function relationships of the dicopper enzymes.[18,19] Spectroscopic features of the model complexes are in good agreement with those of oxy-hemocyanin, catechol oxidase, and tyrosinase, suggesting that dioxygen is bound to the dicopper site as peroxide in a μ-η^2:η^2 side-on bridging mode in these enzymes prior to their X-ray structural analyses. The (μ-η^2:η^2-peroxo)dicopper(II) complexes supported by a variety of tridentate and bidentate nitrogen ligands were reported to provide important information about the effects of the ligand on the structure and physicochemical properties of the dicopper peroxo complexes.[20−23] Lots of reactivity studies on the dicopper peroxo complexes and substrate phenol derivatives demonstrated that C−C coupling dimer products are formed rather than the oxygenation product catechols.[24−31] These results tell us that the reactions of phenols and the dicopper peroxo complexes involve phenolic O−H bond activation to generate stable phenoxyl radicals as intermediates.

Nowadays computational quantum chemistry is of great use in the mechanistic analysis of metalloenzymes. Siegbahn and Wirstram[32] showed using density functional theory (DFT) calculations that the bis(μ-oxo) $Cu^{III}Cu^{III}$ state should not be involved in the catalytic mechanism of tyrosinase because the bis(μ-oxo) $Cu^{III}Cu^{III}$ state lies above the μ-η^2:η^2 peroxo $Cu^{II}Cu^{II}$ state in energy. Moreover, Siegbahn[33] showed that dioxygen attacks the phenolate ring, which is then followed by O−O bond cleavage. In the latter study a calculation model with five imidazole ligands for histidine and one water ligand was set up on the basis of limited structural information about tyrosinase at that time. We have now better structural information for reasonably developing a quantum chemical study for the catalysis of tyrosinase. Moreover, we are able to perform quantum mechanical/molecular mechanical (QM/MM) calculations, which can reasonably take important effects of surrounding amino-acid residues, hydrogen bonding, and protein environment into account. Under these situations, we decided to study the mechanism for the biological conversion of tyrosine to dopaquinone on the basis of whole enzyme calculations to throw light on a recent mechanistic proposal[1] for this enzyme from a different point of view.

Figure 1 shows an X-ray crystal structure of the oxy form of tyrosinase (Protein Data Bank code 1WX2). This crystal structure analysis of tyrosinase was successfully done together with ORF378, a tyrosine residue of which extends to the substrate-binding pocket and shields the catalytically active

(14) (a) Jolley, R. L., Jr.; Evans, L. H.; Mason, H. S. *Biochem. Biophys. Res.* **1972**, *46*, 878. (b) Jolley, R. L., Jr.; Evans, L. H.; Makino, N.; Mason, H. S. *J. Biol. Chem.* **1974**, *249*, 335.
(15) Jackman, M. P.; Hajnal, A.; Lerch, K. *Biochem. J.* **1991**, *274*, 707.
(16) van Gelder, C. W. G.; Flurkey, W. H.; Wichers, H. J. *Phytochemistry* **1997**, *45*, 1309.
(17) Rodríguez-López, J. N.; Tudela, J.; Varón, R.; García-Carmona, F.; García-Cánovas, F. *J. Biol. Chem.* **1992**, *267*, 3801.
(18) Blackburn, N. J.; Strange, R. W.; Farooq, A.; Hake, M. S.; Karlin, K. D. *J. Am. Chem. Soc.* **1988**, *110*, 4263.
(19) (a) Kitajima, N.; Fujisawa, K.; Moro-oka, Y. *J. Am. Chem. Soc.* **1989**, *111*, 8975. (b) Kitajima, N.; Fujisawa, K.; Fujimoto, C.; Moro-oka, Y.; Hashimoto, S.; Kitagawa, T.; Toriumi, K.; Tatsumi, K.; Nakamura, A. *J. Am. Chem. Soc.* **1992**, *114*, 1277.
(20) Mirica, L. M.; Ottenwaelder, X.; Stack, T. D. P. *Chem. Rev.* **2004**, *104*, 1013.
(21) Lewis, E. A.; Tolman, W. B. *Chem. Rev.* **2004**, *104*, 1047.
(22) Hatcher, L. Q.; Karlin, K. D. *Adv. Inorg. Chem.* **2006**, *58*, 131.
(23) Itoh, S.; Fukuzumi, S. *Acc. Chem. Res.* **2007**, *40*, 592.
(24) Kitajima, N.; Koda, T.; Iwata, Y.; Moro-oka, Y. *J. Am. Chem. Soc.* **1990**, *112*, 8833.
(25) Paul, P. P.; Tyeklár, Z.; Jacobson, R. R.; Karlin, K. D. *J. Am. Chem. Soc.* **1991**, *113*, 5322.
(26) Mahapatra, S.; Halfen, J. A.; Wilkinson, E. C., Jr.; Tolman, W. B. *J. Am. Chem. Soc.* **1994**, *116*, 9785.
(27) Obias, H. V.; Lin, Y.; Murphy, N. N.; Pidcock, E.; Solomon, E. I.; Ralle, M.; Blackburn, N. J.; Neuhold, Y.-M.; Zuberbühler, A. D.; Karlin, K. D. *J. Am. Chem. Soc.* **1998**, *120*, 12960.
(28) Halfen, J. A.; Young, V. G., Jr.; Tolman, W. B. *Inorg. Chem.* **1998**, *37*, 2102.
(29) Mahadevan, V.; DuBois, J. L.; Hedman, B.; Hodgson, K. O.; Stack, T. D. P. *J. Am. Chem. Soc.* **1999**, *121*, 5583.
(30) Mahadevan, V.; Henson, M. J.; Solomon, E. I.; Stack, T. D. P. *J. Am. Chem. Soc.* **2000**, *122*, 2890.
(31) Osako, T.; Ohkubo, K.; Taki, M.; Tachi, Y.; Fukuzumi, S.; Itoh, S. *J. Am. Chem. Soc.* **2003**, *125*, 11027.
(32) Siegbahn, P. E. M.; Wirstam, M. *J. Am. Chem. Soc.* **2001**, *123*, 11819.
(33) Siegbahn, P. E. M. *J. Biol. Inorg. Chem.* **2003**, *8*, 567.

Scheme 1

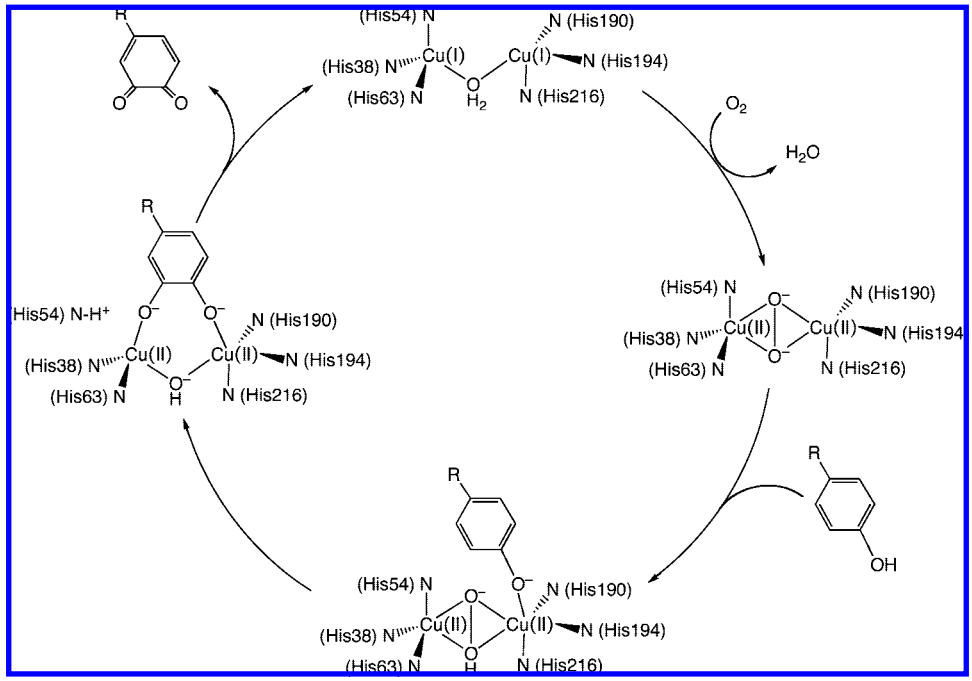

dicopper site. After dissociation of this caddie protein, the active site is accessible to substrates. It is therefore reasonable to remove the ORF378 moiety in our QM/MM calculations. In view of the crystal structure, one histidine residue (His54) that coordinates to CuA comes from a protein loop while the other five histidine residues (His38, His63, His190, His194, and His216) come from surrounding α-helix structures. Matoba et al.[1] propose that the His54 residue should act as a catalytic base because of the flexibility of the loop structure. We would like to turn our attention to this statement on the basis of detailed QM/MM calculations.

A proposed tyrosinase-specific catalytic mechanism is shown in Scheme 1.[1] The (μ-η^2:η^2-peroxo)dicopper(II) species plays an essential role in a series of elementary processes mediated by the dicopper species of tyrosinase. A proton is abstracted from the phenolic O−H bond of tyrosine. The resultant phenoxo ion binds to the right-side copper ion at the sixth coordination site. In the final stages of the catalysis, one of the histidine ligands (His54) acts as a catalytic base for the deprotonation from substrate. However, there are missing links in the catalytic cycle particularly in the multistep reactions between the binding of tyrosine to the dicopper site and the release of dopaquinone, we think. On the basis of computational quantum chemistry, we consider the reaction mechanism for the biological conversion of tyrosine to dopaquinone in detail from structural and energetic points of view in this study.

Computational Details

Tyrosinase−Substrate Complex. A model of tyrosinase−substrate complex was prepared on the basis of the crystal structure of the oxy form of tyrosinase determined by X-ray diffraction at a resolution of 1.80 Å, as shown in Figure 1.[1,34,35] Here we removed ORF378 that prevents substrate tyrosine to access the dicopper active site of tyrosinase and added hydrogen atoms and substrate tyrosine to the crystal structure. An initial geometry was obtained from the crystal structure (EC 1.14.18.1) by removal of ORF378 and neighboring water molecules. Hydrogen atoms were added on the basis of the geometry specified in the residue database on Discovery Studio 2.0.[36] The hydrogen atoms were first relaxed by using steepest descent minimization with the peptide held fixed, and then tyrosine was added in the neighborhood of the dicopper site. After the insertion of tyrosine, we optimized the whole MM region to obtain a starting structure for MD calculations. The system was heated and equilibrated with CHARMm;[37] in the MD calculations a time step of 1 fs was used. The initial temperature was set to be 50 K, which was raised to 300 K with the Berendsen method during the 2 ps of equilibration. A production run was then carried out for another 10 ps at 300 K. During the MD calculations, the coordinates of the QM-region atoms were kept fixed. Finally, the system was minimized with the adopted basis Newton−Raphson algorithm. The ball-and-stick representation in Figure 1 indicates atoms in the QM region, and the ribbon representation indicates atoms in the MM region. The charge of the QM region is +2, and that of the MM region is counted to be −4; as a result, the total charge of the entire system is −2. The atomic charges of amino acid residues in the MM region were assigned on the basis of the atomic parameters of the Amber force field (Amber96).[38] The substrate-binding pocket and the surface charge distribution in the QM/MM model are shown in Figure 2. The positive charge of the QM region is compensated by the neighboring Asp45 and Glu182 residues in the MM region (not explicitly shown here). The total charge of −2 in this large molecular system would have little effect on the structures and energy profile of the reaction pathway.

Method of Calculation. Three-dimensional models for the tyrosinase−substrate complex were optimized with the two-layer ONIOM (IMOMM) method,[39] implemented in the Gaussian 03 program package.[40] In the QM/MM calculations we defined the active center of tyrosinase as a QM region (100 atoms), and the rest of the enzyme as an MM region. Our model shown in Figure 3 consists of 4886 atoms in total. The QM region includes two copper atoms (CuA and CuB), a dioxygen molecule bound to the dicopper site as peroxide, six histidine residues (His38, His54,

(34) Decker, H.; Schweikardt, T.; Tuczek, F. *Angew. Chem., Int. Ed.* **2006**, *45*, 4546.
(35) Decker, H.; Schweikardt, T.; Nillius, D.; Salzbrunn, U.; Jaenicke, E.; Tuczek, F. *Gene* **2007**, *398*, 183.
(36) *Discovery Studio 2.0*; Accelrys Software Inc.: San Diego, 2007.
(37) Brooks, B. R.; Bruccoleri, R. E.; Olafson, B. D.; States, D. J.; Swaminathan, S.; Karplus, M. *J. Comput. Chem.* **1983**, *4*, 187.

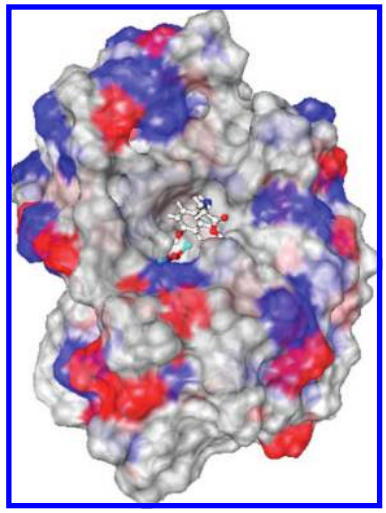

Figure 2. Substrate-binding pocket and molecular surface of charge distribution in the QM/MM model. Red and blue show the negative (Asp and Glu) and positive (Lys and Arg) charge distributions, respectively.

His63, His190, His194, and His216), and substrate tyrosine. The QM region can describe the essential bond-cleavage and -formation processes in the enzyme while the MM region can promote interactions with the QM region through partial charges, hydrogen bonding, and van der Waals forces of atoms in the MM region. The link atoms used in the QM/MM border are marked by star, as indicated in Figure 3 (right), where the C−H(QM)/C−C(MM) ratio adopted is 0.7239. The starred atoms were replaced by hydrogen atoms in the QM part of the QM/MM calculation. These artificial hydrogen atoms (called capping atoms or link atoms) were placed along the broken bond between a QM atom and an MM atom, and the distance from the QM atom to the link hydrogen was taken as 0.7239 times the MM bond distance of the bond broken (because this is the ratio of normal C−H and C−C bond lengths). We used the B3LYP method[41] for QM calculations with the m6−31G* basis set,[42] which modifies the 6−31G* basis set for the first-row transition metals, for the copper atoms, the 6−31+G* basis set[43] for the oxygen atoms, and the 6−31G* basis[43a,b,45] set for other atoms. All calculations were done in the singlet state within the framework of the broken-symmetry methodology. The method of choice for MM calculations is the Amber96 force field.[38]

We first calculated the oxy form of tyrosinase without substrate to evaluate the reliability of our choice of calculation. Figure 4 shows a QM/MM optimized active site structure superimposed on the X-ray crystal structure of the oxy form of tyrosinase. The formal charge of each copper ion is reasonably counted to be +2; and therefore, this is a μ-η^2:η^2 peroxo $Cu^{II}Cu^{II}$ structure. Calculated Mulliken atomic spin densities of CuA and CuB are 0.50 and −0.52, respectively, in the broken-symmetry singlet state. The Cu−Cu and O−O distances were optimized to be 3.436 and 1.414 Å, respectively. The QM/MM optimized Cu−Cu and O−O distances are in good agreement with 3.476 and 1.484 Å, respectively, determined by the X-ray structural analysis. Thus, the QM/MM optimized structure and the X-ray structure are very similar, the superimposed backbone atoms of carbon, nitrogen, two copper, and two oxygen atoms having a root-mean-square deviation of 0.800 Å. The optimized structure of the active site of the resting state is fully consistent with the X-ray structure with respect to the coordination spheres. Stable structures corresponding to the reactant, intermediates, and product were fully optimized without geometrical constraint. To estimate the activation energies for transition states in a similar way in the previous studies,[45] we scanned the potential energy surface with fine steps along a selected reaction coordinate using partial geometry optimization. We performed vibrational analyses for the transition states thus obtained to confirm that an optimized geometry corresponds to a saddle point that has only one imaginary frequency.

Results and Discussion

Much effort on the basis of the heavy QM/MM calculations was made to determine the reaction pathway from tyrosine to dopaquinone. The mechanism we propose for the catalytic function of tyrosinase is summarized in Scheme 2. When substrate tyrosine comes into contact with the μ-η^2:η^2 peroxo $Cu^{II}Cu^{II}$ site, one of the Cu−O bond is cleaved while the O−O bond remains unchanged, and then the O−H bond of tyrosine is cleaved by the resultant Cu−O species. At the same time, the resulting phenoxo ligand is bound to a copper ion. The O−O bond is subsequently cleaved while phenoxyl radical is released from the copper site. After the O−O bond cleavage, the bridging oxygen species attacks an *ortho* position of the benzene ring. In the final stages of the reaction, dopaquinone is formed under the involvement of a histidine residue that comes from a flexible loop structure.

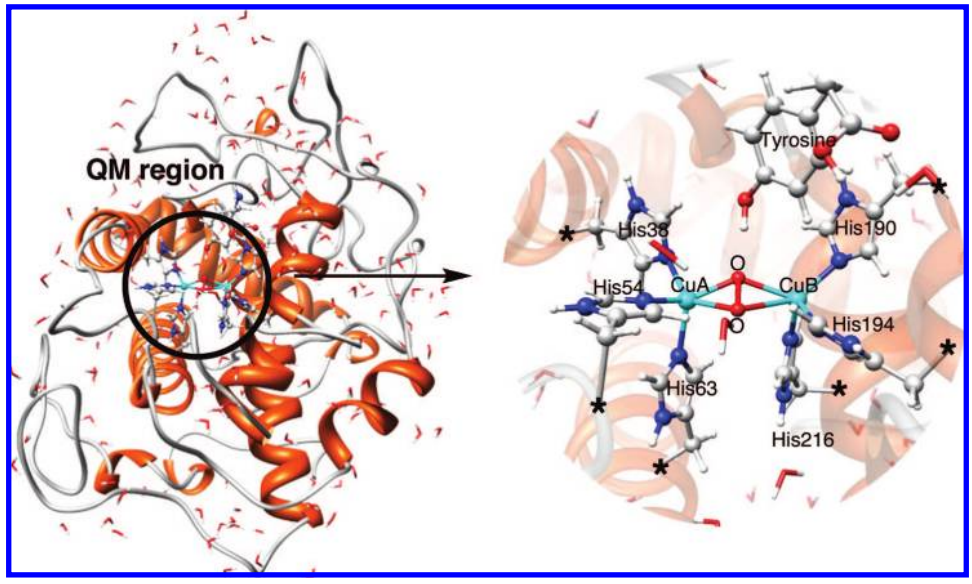

Figure 3. Tyrosinase−substrate complex model with 4886 atoms.

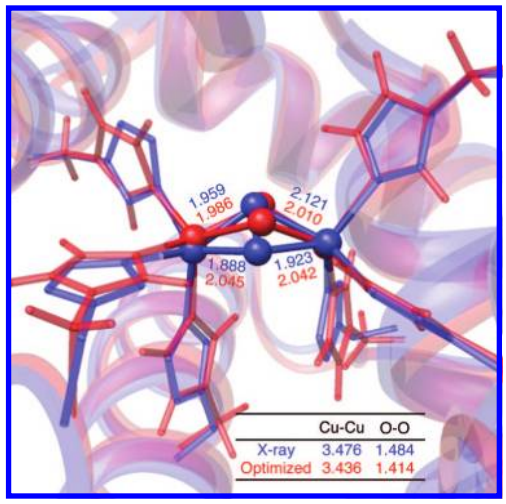

Figure 4. Superimposed structures for the oxy form of tyrosinase. X-ray structure (blue) and QM/MM optimized structure (red).

Thus, the overall reaction consists of five elementary reactions; a computed energy diagram is shown in Figure 5. The energy profile is quite reasonable as a biochemical process that occurs under physiological conditions because the energy barriers for the transition states are less than 15 kcal/mol. The rate-determining step is found to be the O−O bond cleavage step with an activation energy of 14.9 kcal/mol. We show each step in detail in the following sections.

Proton Transfer from the Phenolic O−H Bond to Dioxygen. Let us first look at the initial tyrosinase−substrate complex **1** shown in Figure 6. We created this tyrosinase−substrate complex by inserting substrate tyrosine to the μ-η^2:η^2 peroxo $Cu^{II}Cu^{II}$ site. As a result, the coordination of the dioxygen molecule is changed from the μ-η^2:η^2 peroxo form to a μ-η^1:η^2 peroxo form while the O−O bond distance of 1.414 Å remains unchanged. This geometrical transformation plays an important role in the subsequent proton transfer from tyrosine to dioxygen. As a result of the CuB−O1 bond dissociation, the resultant CuA−O1 species activates the phenolic O−H bond and then abstracts the proton from tyrosine. The distance between the two copper ions increases from 3.436 to 3.886 Å during this process. Calculated Mulliken atomic spin densities of CuA and CuB in **1** are 0.44 and −0.57 in the broken-symmetry singlet state, respectively. The distance of the CuB−O3 bond is 2.316 Å; this long bond means that this interaction is weak.

The proton transfer occurs via **TS1**, leading to the formation of the μ-η^1:η^2 hydroperoxo intermediate **2**. This transition state involves an O1−H bond of 1.145 Å and an O3−H bond of 1.267 Å. These bond distances are reasonable for a transition state structure responsible for the cleavage of an O−H bond and the formation of an O−H bond. This process, which requires an activation energy of 2.4 kcal/mol, is expected to take place easily to form intermediate **2**. The energy of **2** is 1.4 kcal/mol relative to **1**. The O1−O2 bond distance of 1.414 Å in the peroxo species **1** is increased to 1.440 Å in the hydroperoxo species **2** because of the protonation of the O1 atom, while the O−O bond is still retained in the course of this reaction. The increase in the O−O distance has a significant effect on the lowering of the activation energy for the subsequent O−O bond dissociation step. These geometrical changes decrease the CuB−O3 bond from 2.316 Å in **1** to 2.023 Å in **2**.

O−O Bond Dissociation of the Hydroperoxo Species. A subsequent O−O bond dissociation via **TS2** results in the formation of intermediate **3**, as shown in Figure 7. **TS2** is a transition state, in which the O1−O2 bond dissociation takes place concomitantly with the CuB−O1 bond formation and the CuB−O3 bond dissociation. The O1−O2, CuB−O1, and CuB−O3 distances in **3** are 1.735, 1.984, and 4.200 Å, respectively. Furthermore, the bond between CuA and the ϵ-N atom of His63 is dissociated while the ϵ-N atom forms a hydrogen bond with the O1−H group. This is caused by the rotation of O1 and O2. A calculated activation barrier for this O−O bond dissociation step is 14.9 kcal/mol, and the energy of **TS2** lies 16.3 kcal/mol relative to **1**, **TS2** being the highest peak in energy profile along the proposed reaction pathway, as shown in Figure 5. We consider this O−O bond dissociation to be the rate-determining step in the biological conversion of tyrosine to dopaquinone. In a previous DFT study,[33] the O−O dissociation step was calculated to be endothermic by 23 kcal/mol, and therefore, this mechanism was ruled out in the catalysis of

Scheme 2

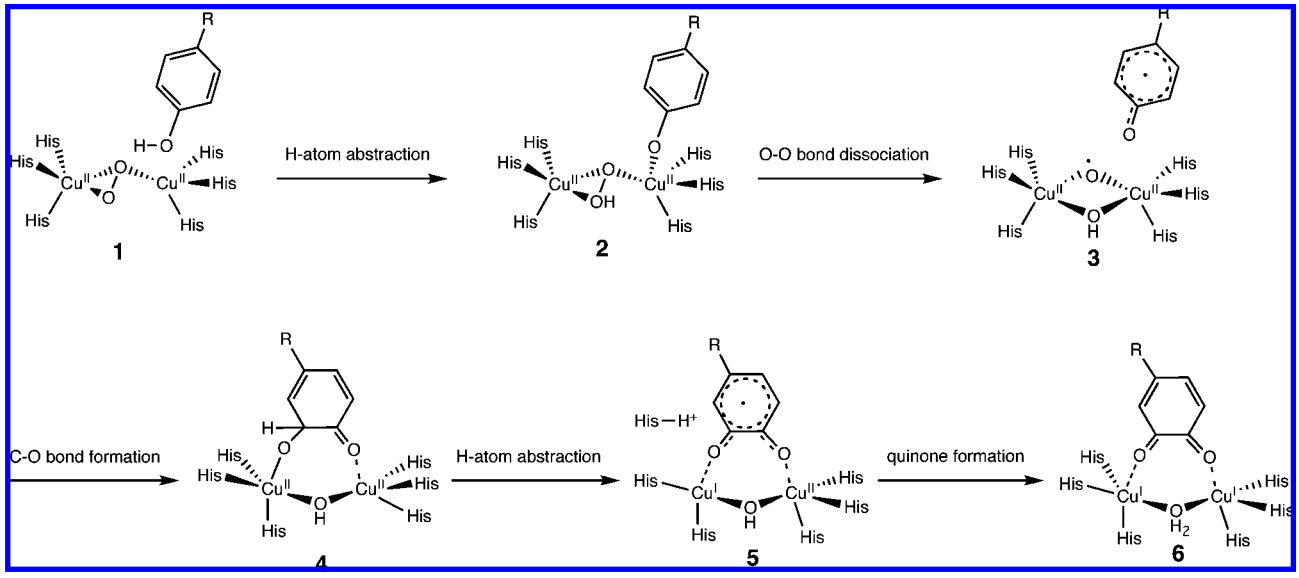

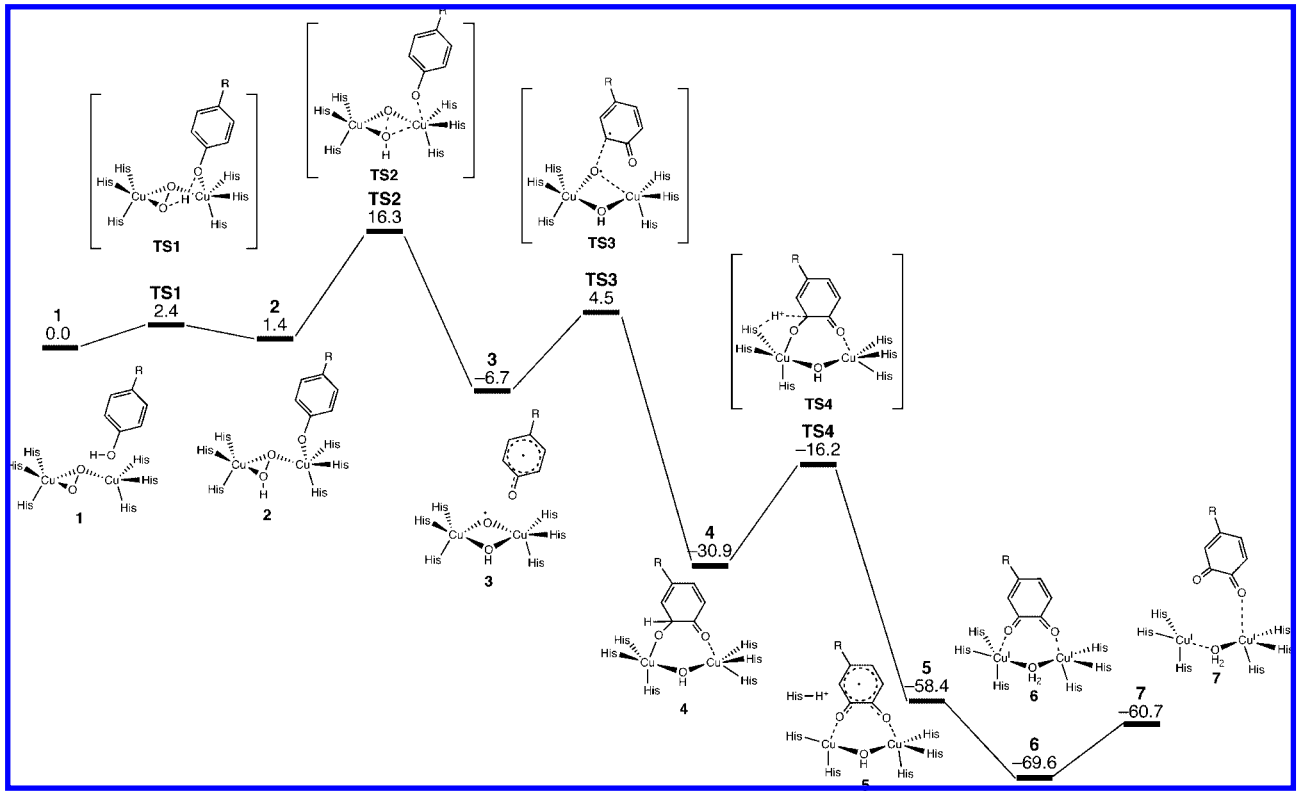

Figure 5. Energy diagram for the conversion of tyrosine to dopaquinone. Energies in kcal/mol.

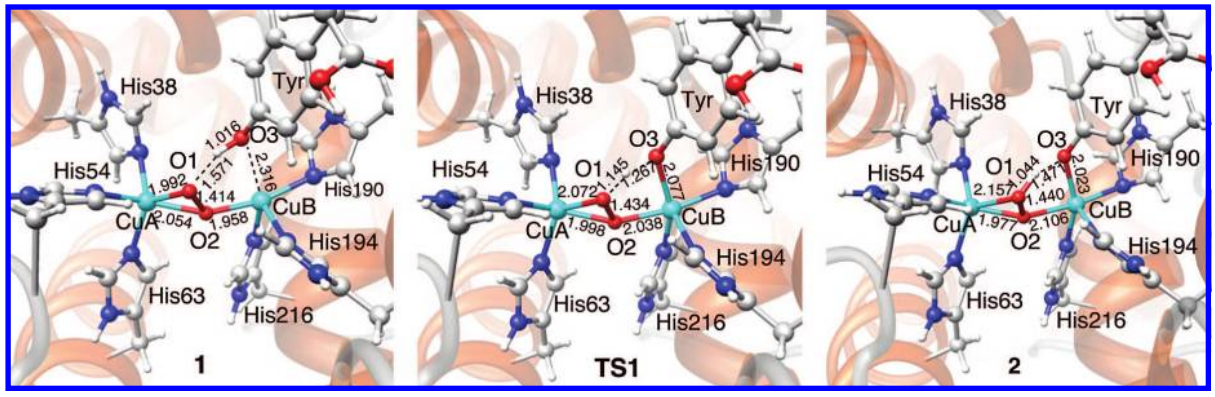

Figure 6. QM/MM optimized structures for the initial proton-transfer step. **TS1** has one imaginary vibrational mode of 503.6i cm^{-1}.

tyrosinase. It was proposed that dioxygen attacks the phenolate ring which is then followed by O−O bond cleavage. This mechanistic difference comes from different dioxygen species considered in the catalysis. In the previous study, the O−O dissociation of a "dicopper peroxo" species was considered and calculated, whereas in the present mechanism that of a "dicopper hydroperoxo" species is proposed. In our mechanism, the initial peroxo species is protonated as a result of the heterolysis of the phenolic O−H bond of tyrosine; therefore, the O−O(H) bond in the hydroperoxo species **2** is significantly activated. Since the O−O(H) bond is weak in comparison with the peroxo O−O bond, our computational result is reasonable. In fact, the O−O bond distance of **1** (peroxo) is significantly increased in **2** (hydroperoxo), as mentioned in the previous section. It is reasonable to consider that the increase in the O−O distance in **2** causes the lowering of the activation energy for the subsequent O−O bond dissociation step. Calculated Mulliken atomic spin densities of O2 and the tyrosine moiety in intermediate **3** are 0.76 and −0.99, respectively. Thus, the O−O bond dissociation results in the formation of copper−oxygen radical and phenoxyl radical. These radical species are coupled to form a C−O bond at an *ortho* position of the benzene ring in the following reaction step. Note that the stable phenoxyl radical plays an essential role in the proposed reaction pathway and that this radical coupling is well regulated in the protein environment. Involvement of phenoxyl radical is also suggested in the chemistry of dicopper model complexes because C−C coupling dimer products are observed in extensive reactivity studies.[24−31]

(38) Cornell, W. D.; Cieplak, P.; Bayly, C. I.; Gould, I. R.; Merz, K. M., Jr.; Ferguson, D. M.; Spellmeyer, D. C.; Fox, T.; Caldwell, J. W.; Kollman, P. A. *J. Am. Chem. Soc.* **1995**, *117*, 5179.
(39) (a) Maseras, F.; Morokuma, K. *J. Comput. Chem.* **1995**, *16*, 1170. (b) Svensson, M.; Humbel, S.; Froese, R. D. J.; Matsubara, T.; Sieber, S.; Morokuma, K. *J. Phys. Chem.* **1996**, *100*, 19357. (c) Vreven, T.; Morokuma, K. *J. Comput. Chem.* **2000**, *21*, 1419.

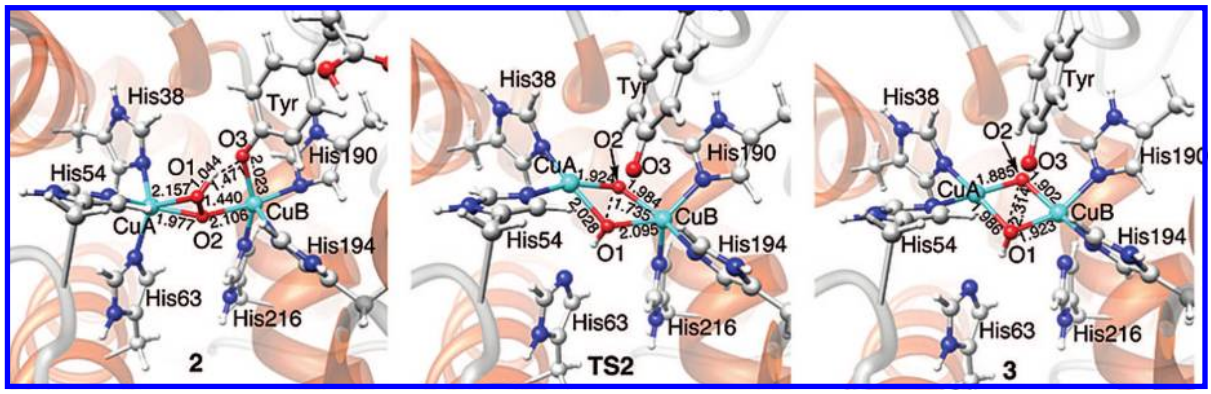

Figure 7. QM/MM optimized structures for the O−O bond dissociation step. **TS2** has one imaginary vibrational mode of 613.3i cm^{-1}.

Table 1. Calculated Reaction Rates at 298 K as a Function of Activation Energy (ΔE)

ΔE (kcal/mol)	k (s^{-1})
10	$2.89 \times 10^{+5}$
11	$5.34 \times 10^{+4}$
12	$9.87 \times 10^{+3}$
13	$1.82 \times 10^{+3}$
14	$3.37 \times 10^{+2}$
15	$6.23 \times 10^{+1}$
16	$1.15 \times 10^{+1}$
17	$2.13 \times 10^{\circ}$
18	3.93×10^{-1}
19	7.26×10^{-2}
20	1.34×10^{-2}

We characterized this rate-determining step in the catalytic cycle of tyrosinase by calculating the reaction rate with transition state theory.[46] Table 1 summarizes calculated reaction rates at 298 K as a function of activation energy. Rodríguez-López et al.[17] reported the reaction rate for the *o*-hydroxylation of monophenols by tyrosinase to be 10^3 s^{-1}. In view of Table 1, we estimate that this value should correspond to the activation energy of 13−14 kcal/mol, which is in excellent agreement with a calculated value of 14.9 kcal/mol for **TS2**. Thus, the reaction pathway we propose is reasonable from the point of view of reaction rate.

C−O Bond Formation at an *Ortho* Position of the Benzene Ring. As shown in Figure 8, the O2 atom attacks the benzene ring of tyrosine via **TS3**, in which the radical coupling reaction is clearly of *ortho* selectivity. This selectivity is reasonably explained by the spin-density distribution. In fact, a calculated spin density of O2 is 0.76, and those of the *ortho* and *meta* positions are −0.28 and 0.14, respectively. The C−O2 distance in **TS3** is computed to be 2.300 Å. This radical coupling increases the distance of the CuB−O2 bond from 1.902 Å in intermediate **3** to 2.051 Å and decreases that of the CuB−O3 bond from 3.957 Å in **3** to 3.581 Å in **TS3**, resulting in the CuB−O2 bond dissociation and the CuB−O3 bond formation. The activation energy of **TS3** is computed to be 11.2 kcal/mol; thus, it is accessible under physiological conditions. Intermediate **4** has a 7-membered ring at the dicopper active site. There are no spin densities at O1 and in the tyrosine moiety of intermediate **4** because of the occurrence of the radical coupling. The C−O2 bond changes from 2.300 Å in **TS3** to 1.369 Å in **4**. The energy of intermediate **4** is −24.2 kcal/mol relative to intermediate **3**. The C−H bond distance of 1.129 Å is longer than the C−H bond distance of 1.078 Å in **TS3**. In the next step, this H atom is considered to shift to the ϵ-N atom of His54 as proton.

Proton Transfers Mediated by His54 and Dopaquinone Formation. As shown in Figure 9, the His54 residue abstracts the H-atom as proton from an *ortho* position of the benzene ring via **TS4**, resulting in the formation of intermediate **5**. This reaction leads to the dissociation of the CuA−N bond. The proton of tyrosine shifts to the ϵ-N atom of His54, which is considered to play a role as a general base. The ϵ-N−H and C−H distances are reasonably computed to be 1.440 and 1.362 Å, respectively, in **TS4**. The activation energy of **TS4** is computed to be 14.7 kcal/mol, which is higher than the other proton abstraction of 2.4 kcal/mol in **TS1** because the dissociation of the CuA−ϵ-N bond is involved in the later process. Although the activation energy of this step is comparable to that of **TS2**, **TS4** lies 16.2 kcal/mol below **1**; therefore, the driving force for this reaction via **TS4** is considered to be larger.

In intermediate **5**, the C−O1 and C−O3 bond distances are 1.291 and 1.292 Å, respectively, and the CuA−O1 and CuB−O3 bond distances are 2.190 and 2.114 Å, respectively. Computed Mulliken atomic spin densities of O1, O3, CuA, and CuB are 0.19, 0.10, 0.05, and −0.61, respectively. These results tell us that one electron of the phenyl group is transferred to CuA, resulting in the formation of dopaquinone radical anion. Another electron transfer from dopaquinone radical anion needs to form neutral dopaquinone. Finally, intermediate **5** releases the proton from His54 to the hydroxo ligand that bridges between CuA and CuB, resulting in the formation of the product complex **6**. One water molecule is formed by the shift of the proton to the hydroxo ligand. Simultaneously, electron transfer occurs between CuB and dopaquinone radical anion, resulting in the formation of dopaquinone. The formal charge of the two copper atoms is changed from Cu^{II} to Cu^{I} in the final stages of the reaction. Therefore, we consider **6** to be in the closed-shell singlet state. This step requires no activation barrier and takes place easily to form the product complex **6**. The release of dopaquinone, which requires 8.9 kcal/mol relative to **6**, reproduces the deoxy form of tyrosinase. The exchange of a water ligand bound to CuA and CuB and a dioxygen molecule is needed to complete the catalytic cycle for the conversion of tyrosine to dopaquinone. The direct pathway from intermediate **4** to the product complex **6** without participation of the His54 residue is less reasonable because the H···OH distance of 3.439 Å is larger than the H···N(His54) distance of 3.173 Å in **4**. Despite our best efforts, we could not reasonably locate the transition state for the direct pathway.

Concluding Remarks

On the basis of the recent X-ray crystal analysis of tyrosinase, we have discussed a possible mechanism for the biological

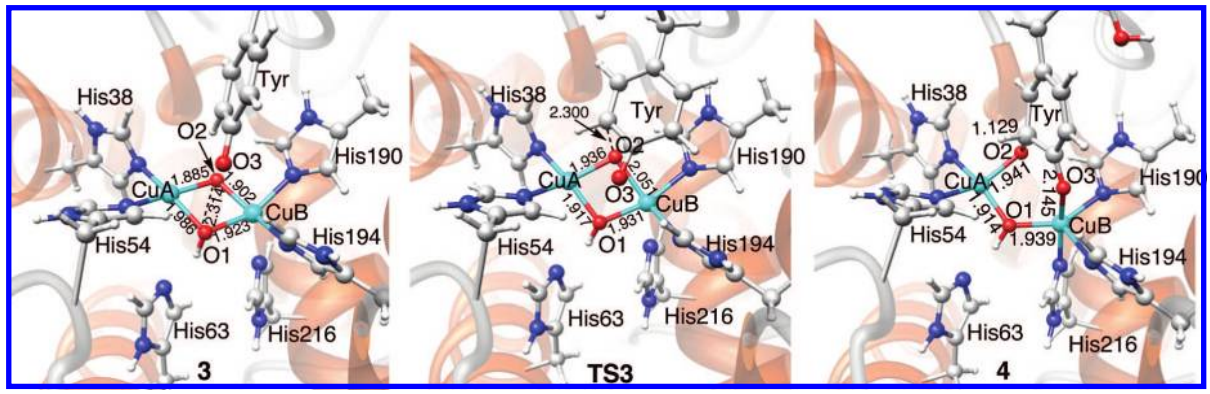

Figure 8. QM/MM optimized structures for the C−O bond formation step. **TS3** has one imaginary vibrational mode of 244.0i cm^{-1}.

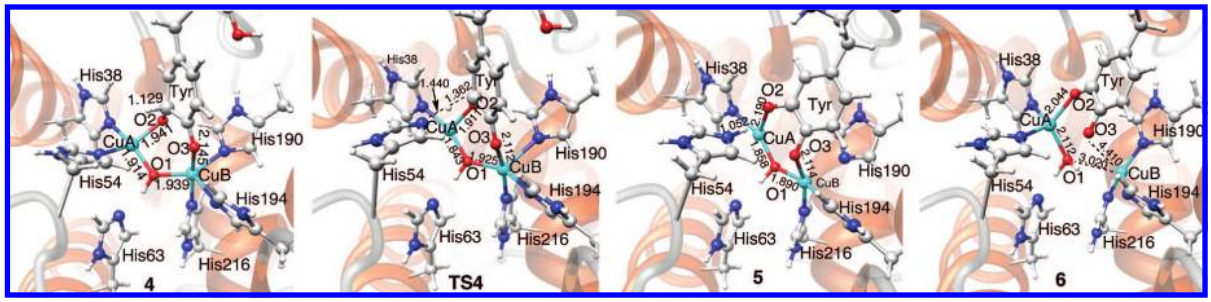

Figure 9. QM/MM optimized structures for the quinone formation step. **TS4** has one imaginary vibrational mode of 1321.6i cm^{-1}.

conversion of tyrosine to dopaquinone using QM/MM calculations, which can reasonably take environmental effects into account. Our QM/MM study supports the recent mechanistic proposal on the enzymatic function of tyrosinase.[1] The (μ-η^2:η^2-peroxo)dicopper(II) species plays a central role in the catalysis of tyrosinase. Stable phenoxyl radical is involved in the reaction pathway. The mechanism is in contrast to those for C−H bond activation by particulate methane monooxygenase, in which the bis(μ-oxo)$Cu^{II}Cu^{III}$ species is proposed to convert methane to methanol,[47] and by peptidilglycine α-hydroxylating monooxygenase and dopamine β-monooxygenase, in which either mononuclear copper(II)−superoxo species[48] or copper(III)−oxo (copper(II)−O•) species[49,50] is proposed to play a role in the hydroxylation. A series of tyrosinase reactions involve five steps of proton transfer from the phenolic O−H bond to the dioxygen moiety, O−O bond dissociation of the hydroperoxo species, C−O bond formation at an *ortho* position of the benzene ring, proton migrations mediated by His54, and quinone formation. The energy profile of the calculated reaction pathway is reasonable as elementary processes that occur under physiological conditions. Detailed analyses of the energy profile demonstrate that the O−O bond dissociation is the rate-determining step. On the basis of the proposal of Matoba et al.[1] we demonstrated that the His54 residue, which is flexible because of a loop structure in the protein, would play a role as a general base in the proton migrations in the final stages of the reaction. The activation energy for the O−O bond dissociation is computed to be 14.9 kcal/mol, which is in good agreement with a measured kinetic constant ($k = 10^3$ s^{-1}).[17]

Acknowledgment. K.Y. thanks Grants-in-Aid for Scientific Research (nos. 18350088, 18066013, and 18GS0207) from the Japan Society for the Promotion of Science, the Global COE Project, the Nanotechnology Support Project, the Joint Project of Chemical Synthesis Core Research Institutions from the Ministry of Culture, Sports, Science, and Technology of Japan (MEXT), and CREST of the Japan Science and Technology Cooperation.

Supporting Information Available: Complete ref 40 and atomic Cartesian coordinates for all the structures optimized in the present study. This material is available free of charge via the Internet at http://pubs.acs.org.

JA802618S

(40) Frisch, M. J.; et al. *Gaussian 03*, revision C.02; Gaussian, Inc.: Wallingford, CT, 2004.
(41) (a) Becke, A. D. *Phys. Rev. A* **1988**, *38*, 3098. (b) Becke, A. D. *J. Chem. Phys.* **1993**, *98*, 5648. (c) Lee, C.; Yang, W.; Parr, R. G. *Phys. Rev. B* **1988**, *37*, 785. (d) Vosko, S. H.; Wilk, L.; Nusair, M. *Can. J. Phys.* **1980**, *58*, 1200. (e) Stephens, P. J.; Devlin, F. J.; Chabalowski, C. F.; Frisch, M. J. *J. Phys. Chem.* **1994**, *98*, 11623.
(42) (a) Rassolov, V. A.; Pople, J. A.; Ratner, M. A.; Windus, T. L. *J. Chem. Phys.* **1998**, *109*, 1223. (b) Mitin, A. V.; Baker, J.; Pulay, P. *J. Chem. Phys.* **2003**, *118*, 7775.
(43) (a) Hehre, W. J.; Ditchfield, R.; Pople, J. A. *J. Chem. Phys.* **1972**, *56*, 2257. (b) Hariharan, P. C.; Pople, J. A. *Theor. Chim. Acta* **1973**, *28*, 213. (c) Clark, T.; Chandrasekhar, J.; Spitznagel, G. W.; Schleyer, P. v. R. *J. Comput. Chem.* **1983**, *4*, 294.
(44) Ditchfield, R.; Hehre, W. J.; Pople, J. A. *J. Chem. Phys.* **1971**, *54*, 724.
(45) (a) Kamachi, T.; Toraya, T.; Yoshizawa, K. *J. Am. Chem. Soc.* **2004**, *126*, 16207. (b) Kamachi, T.; Toraya, T.; Yoshizawa, K. *Chem. Eur. J.* **2007**, *13*, 7864.
(46) Frost, A. A.; Pearson, R. G. *Kinetics and Mechanism*; Wiley: New York, 1961.
(47) (a) Yoshizawa, K.; Suzuki, A.; Shiota, Y.; Yamabe, T. *Bull. Chem. Soc. Jpn.* **2000**, *73*, 815. (b) Yoshizawa, K.; Shiota, Y. *J. Am. Chem. Soc.* **2006**, *128*, 9873.
(48) Chen, P.; Solomon, E. I. *J. Am. Chem. Soc.* **2004**, *126*, 4991.
(49) Yoshizawa, K.; Kihara, N.; Kamachi, T.; Shiota, Y. *Inorg. Chem.* **2006**, *45*, 3034.
(50) Crespo, A.; Martí, M. A.; Roitberg, A. E.; Amzel, L. M.; Estrin, D. A. *J. Am. Chem. Soc.* **2006**, *128*, 12817.